



Interannual variability of western North Pacific SST anomalies and its impact on North Pacific and North America

Jae-Heung Park^{1,2} · Soon-II An² · Jong-Seong Kug¹

Received: 9 September 2016 / Accepted: 16 January 2017 / Published online: 17 February 2017
© Springer-Verlag Berlin Heidelberg 2017

Abstract In this study, the interannual variability of sea surface temperature (SST) and its atmospheric teleconnection over the western North Pacific (WNP) toward the North Pacific/North America during boreal winter are investigated. First, we defined the WNP mode as the first empirical orthogonal function (EOF) mode of SST anomalies over the WNP region ($100\text{--}165^{\circ}\text{E}$, $0\text{--}35^{\circ}\text{N}$), of which the principle component time-series are significantly correlated with several well-known climate modes such as the warm pool mode which is the second EOF mode of the tropical to North Pacific SST anomalies, North Pacific oscillation (NPO), North Pacific gyre oscillation (NPGO), and central Pacific (CP)-El Niño at 95% confidence level, but not correlated with the eastern Pacific (EP)-El Niño. The warm phase of the WNP mode (sea surface warming) is initiated by anomalous southerly winds through reduction of wind speed with the background of northerly mean winds over the WNP during boreal winter, i.e., reduced evaporative cooling. Meanwhile, the atmospheric response to the SST warming pattern and its diabatic heating further enhance the southerly wind anomaly, referred to the wind–evaporation–SST (WES) feedback. Thus, the WNP mode is developed and maintained through winter until spring, when the northerly mean wind disappears. Furthermore, it is also known that anomalous upper-level divergence associated with WNP mode leads to the NPO-like structure

over the North Pacific and the east–west pressure contrast pattern over the North America through Rossby wave propagation, impacting the climate over the North Pacific and North America.

Keywords Western North Pacific (WNP) mode · North Pacific oscillation (NPO) · Wind–evaporation–SST (WES) feedback

1 Introduction

The western North Pacific (WNP), which is seasonally overlapped with the Pacific warm pool, the highest sea surface temperature (SST) region in the world (Fu et al. 1994; Zhang 1993), is a climatologically important place, because its variability is directly connected not only to the tropical region through the Walker circulation but also to the extratropical region through the Hadley circulation (Park and An 2014). Therefore, changes in atmospheric and oceanic environments over the WNP coincidentally influence on climate variability over both the tropics and extratropics. For example, the strengthened surface southerly wind anomalies over the WNP bring warm air into East Asia, leading to a weaker-than-normal East Asian winter monsoon (Wang et al. 2000), and the enhanced atmospheric convection over the WNP pushes the East Asian jet stream to the north, and thus modifies the mid-latitude circulation pattern (Park and An 2014). On the oceanic side, the WNP is a hub of ocean streams, since the main oceanic surface currents, including the Kuroshio and Mindanao currents (Hu and Cui 1991; Jo et al. 2014; Toole et al. 1990) and Indonesian throughflow are connected there, and thus an enormous amount of oceanic heat and mass is imported into the WNP and exported to other tropical and mid-latitude oceans (Lee et al. 2015).

✉ Soon-II An
sian@yonsei.ac.kr

¹ School of Environmental Science and Engineering, Pohang University of Science and Technology (POSTECH), 37673 Pohang, South Korea

² Department of Atmospheric Sciences, Yonsei University, 50 Yonsei-ro, Seodaemun-gu, Seoul 03722, South Korea

The origin of SST variability over the WNP has been widely investigated. Wang et al. (2000) suggested that the westward-propagating Rossby waves at surface level, which is initiated/forced by the central to equatorial SST warming during boreal winter, generate the anticyclonic atmospheric circulation over Philippine Sea. Such anomalous anticyclonic atmospheric circulation, known as Philippine sea anticyclone leads to the northwest-southeast SST contrast with a nodal point near the Philippines by reducing (intensifying) wind speed over the west (east) of Philippines against the climatologically prevailing northerly wind over the WNP in winter. This dipole-type SST anomaly pattern over WNP is expected to be one of the leading SST patterns explaining SST variability in WNP (see Fig. 1b). On the other hand, the mono-pole type SST anomaly pattern, i.e., overall warming (cooling) over WNP (see Fig. 1a) has been frequently shown in previous studies. In these studies, however, the overall warming over WNP was treated as a part of the well-known Pacific climate modes. For example, the warm pool mode (Park et al. 2012), North Pacific gyre oscillation (NPGO) (Bond et al. 2003; Ceballos et al. 2009; Chhak et al. 2009; Di Lorenzo et al. 2008), and the central Pacific (CP)-El Niño (a.k.a. El Niño Modoki, warm pool El Niño, and dateline El Niño) (Larkin and Harrison 2005; Yu and Kao 2007; Ashok et al. 2007; Kao and Yu 2009; Kug et al. 2009) show a common SST configuration over WNP,

that is, the overall warming. It implies that the overall warming over WNP might be related to above mentioned Pacific climate modes in a way that one can be a driving force for another. Nevertheless, there is still a strong possibility that the variability of SST anomalies over WNP can be induced by the internal process, because none of Pacific climate modes can explain whole SST variability of WNP (see Table 1). Despite of its climatological importance, however, the origin of the SST variability over WNP, especially driven by internal process has got paid little attention by climate community.

Meanwhile, SST change/its associated atmospheric convection in the tropical Pacific significantly influences the North Pacific climate via atmospheric teleconnection (e.g., Park et al. 2012, 2014). According to their studies, the atmospheric teleconnection initiated at the tropical western Pacific induces the north–south dipole pressure pattern over the North Pacific, known as North Pacific oscillation (NPO) (Rogers 1981; Linkin and Nigam 2008). At this time, the NPO-related wind stress pattern modifies surface heat fluxes over the North Pacific, which gives rise to NPGO. Thus, the oceanic and atmospheric changes in western tropical Pacific are able to modulate the North Pacific climate. However, there is still lack of understanding on the dynamical mechanism explaining the teleconnection especially that initiated at

Fig. 1 The first two EOF modes and their principal components of SST anomalies over WNP region in boreal winter. They explain 37.4 and 28.3% of the total variability of the SST anomalies, respectively. Contour interval is 0.1 °C

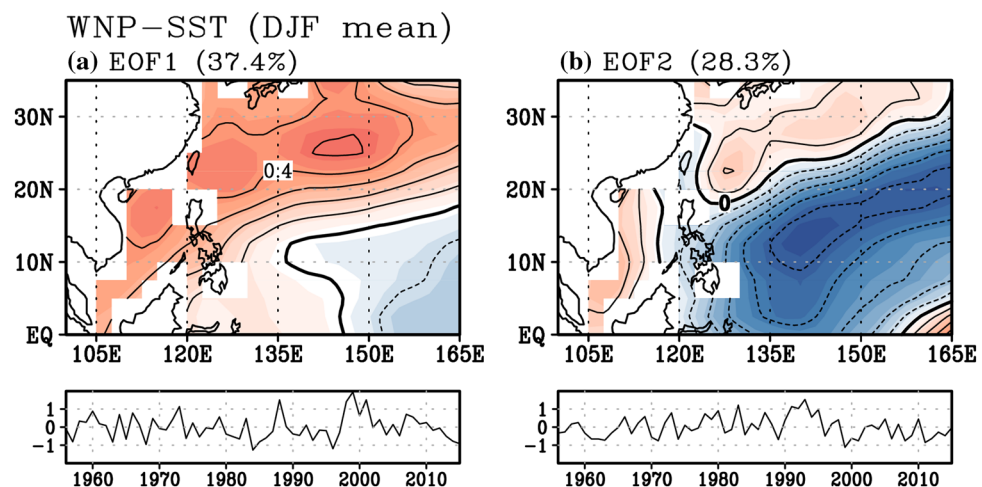


Table 1 Simple linear correlation coefficients of the first two PCs shown in Fig. 1 with other PCs of climate modes

Corr (df 40)	CP-EI Niño	NPGO	NPO	Warm pool	EP-EI Niño	PDO	TBV
1st PC	0.42	0.69	0.6	0.79	0.29	0.1	0.01
2nd PC	0.24	0.024	0.09	0.13	0.71	0.43	0.73

Above 95% confidence level is indicated by bold font. The definition of Each climate mode is like below
PDO & NPGO the first and second EOF mode of North Pacific SST in boreal winter, **NPO** the second EOF mode of North Pacific SLP in boreal winter, **EP-El Niño** the first EOF mode of tropical Pacific SST, **CP-El Niño** the first EOF mode of tropical Pacific SST after removing Niño3 signals, **Warm Pool mode** the second EOF mode of tropical to North Pacific SST, **TBV** the SST difference between the tropical Pacific and the tropical Atlantic

WNP. Therefore, the atmospheric teleconnection mechanism related to the SST variability in WNP needs to be pursued.

The structure of this paper is as follows. The detailed datasets and method are described in the next section. In Sect. 3, the primary mode of the interannual SST variability in the WNP is defined as the WNP mode, and major internal process inducing SST variability of WNP is addressed. The vertical atmospheric structure over the WNP accompanied by the WNP mode and the resultant atmospheric teleconnection toward the North Pacific and to North America are explored in Sect. 4. A summary and discussion are given in the last section.

2 Data

We used National Center for Environmental Prediction Reanalysis 1 (NCEP-R1) monthly data (Kistler et al. 2001) as the main atmospheric data. NCEP-R1 is an assimilated dataset using a state-of-the-art analysis/forecast system covering the period from 1948 to present. The horizontal resolutions are 2.5° in both the zonal and meridional directions, and the vertical resolutions comprise 17 levels. The monthly mean wind field (U_a , V_a , and total wind speed), air temperature, geopotential height (GPH), sea level pressure (SLP), omega (Ω) at 500 hPa for vertical movement, and surface heat fluxes including short wave, long wave, latent and sensible heat were used. We also used ERA-interim reanalysis data from the European Centre for Medium-Range Weather Forecasts (ECMWF). However, both results were almost identical, so we show the results from the NCEP-R1 reanalysis only. For our SST analysis, Extended Reconstruction Sea Surface Temperature Version 3 (ERSSTv3) (Reynolds et al. 2007), which spans the period from 1854 to the present. The ERSSTv3's spatial resolution is 2° in both the zonal and meridional directions. In addition, Global Precipitation Climatology Project version 2.1 (GPCPv2.1) data were also used for the monthly precipitation from 1979 to 2015 (Huffman et al. 2009). Before performing our analysis, all trends were removed, and the climatological mean for 1955–2015 which is the analysis period in this study was also removed, and the winter mean (December to upcoming February, DJF) was essentially taken, since signals are strongest during the boreal winter, so that a total of 60 winter mean yearly data points were created.

3 WNP mode

3.1 Development of WNP mode

In order to identify the dominant mode of SST variability, EOF analysis was applied to the historical SST data

over the WNP during the boreal winter. As presented in Fig. 1, the first two EOF modes explain 37.4 and 28.3% of the total SST variability, respectively. The first EOF mode shows overall warming (or cooling for its opposite phase) over the WNP with a center in the subtropical region between $20\text{--}30^\circ\text{N}$ (Fig. 1a). Meanwhile, the second EOF mode has a well-defined northwest–southeast contrast near Luzon Island (Fig. 1b). In order to confirm the independency of this first EOF mode from El Niño–Southern Oscillation (ENSO) and the robustness, first we linearly removed ENSO signals based on various El Niño indices (Niño3, Niño4, or Niño3.4) from the data, and then applied EOF analysis. It turned out that the spatial pattern of the first EOF mode without ENSO signals (not shown here) was very similar to the original one, and its explained variance was slightly larger. In addition, we limited the period of analysis to recent decades (1979–2015), and the resultant EOF (not shown here) was very similar to the original EOF.

To examine the relationships with other climate modes, the correlations among their principal components (PC) are calculated. The correlation coefficients indicate that the first EOF mode is significantly related to the central Pacific (CP)-El Niño, warm pool mode, NPO, and NPGO at the 95% confidence level (Table 1). On the other hand, the second EOF mode is closely related to the eastern Pacific (EP)-El Niño, Pacific decadal oscillation (PDO) (Mantua et al. 1997), and trans-basin variability (TBV) (Chikamoto et al. 2015), indicating that this mode is considered as a part of conventional ENSO variability as mentioned in Introduction. All the above indices of the climate modes are basically defined using EOF analysis based on the previous studies except for TBV, which is obtained from the equatorial SST difference between the Pacific and Atlantic. Also the CP-El Niño index is taken the principle components of first EOF mode of tropical Pacific SST after linearly removing Niño-3 signals followed by Di Lorenzo et al. (2010). Since the second mode is closely related to the typical ENSO variability as mentioned above (Wang et al. 2000), here we mostly focus on the first mode, and hereafter the corresponding eigen vector and principal component time series are considered as the WNP mode and WNP index for convenience.

To understand the physical processes underlying the WNP mode, we first select eight warm and cold WNP events based on the standard deviation of the WNP index, listed in Table 2. Obviously, the selected events do not match the ENSO events well. In order to understand how such SST warming is developed during the warm period of the WNP mode, composite analysis of the surface heat fluxes including short wave, long wave, latent heat, and sensible heat was conducted (Fig. 2). Each flux is averaged from November to the following January (NDJ).

Table 2 Selected years corresponding to the highest and lowest eight values based on the WNP index

Warm period	1999	1988	2001	1998	1973	1960	1966	2007
Cold period	1984	1996	1968	2015	1963	1985	1957	2014

The order is followed by their strength, from left to right

For the short and long wave radiation fluxes (Fig. 2a–b), opposite patterns with comparable amplitudes indicate offsetting of their effects, which is likely to be related to the clouds over the East China Sea, because clouds reflect incoming short waves and trap the outgoing long waves. Meanwhile, the latent heat and sensible heat fluxes are generally negative during the warm period of the WNP mode (Fig. 2c–d), possibly due to the reduced wind speed (Fig. 3b), and the amplitude of the latent heat fluxes is much stronger. This result indicates that less-than-normal evaporation from the ocean surface gives rise to the SST warming tendency over the WNP (Fig. 3a), which mainly contributes to the SST warming pattern of the WNP mode.

By comparing the surface heat fluxes, we found that the latent heat fluxes play a major role in the development of the WNP mode. The minimum latent heat fluxes (-31 W/m^2) are much smaller than -20 W/m^2 over the WNP. With the assumptions that the averaged mixed layer depth is 75 m (Kara et al. 2003) and that heat dissipation is negligible, the areal averaged latent heat fluxes, -12.9 W/m^2

m^2 , ($120\text{--}160^\circ\text{E}$, $15\text{--}30^\circ\text{N}$, in Fig. 2c) are able to lead to 0.107°C warming over the region (Fig. 2f). Since the SST tendency in the same area in NDJ season, which is obtained from the half of the SST-composite difference between DJF and OND seasons, is 0.135°C (Fig. 2f), thus, temperature warming tendency can be largely explained by the latent heat fluxes during the boreal winter. Relatively, other components such as the short wave, long wave, and sensible heat fluxes play a minor role, and does oceanic heat transport as well (Fig. 2f).

Based on the bulk formulation of latent heat (Eq. 1), two components are essential in generating latent heat fluxes; one is surface wind speed and the other is the specific humidity difference between the ocean surface and the adjacent atmosphere.

$$\text{LE} = L\rho C_{DE} U_r (q_s - q_a(Z_r)) \quad (1)$$

where L is latent heat, $2.5 \times 10^6 \text{ J/kg}$; ρ is air density, 1.293 kg/m^3 ; C_{DE} is the aerodynamic coefficient, 0.003; U_r is wind speed at reference level Z_r ; q_s , and q_a are the

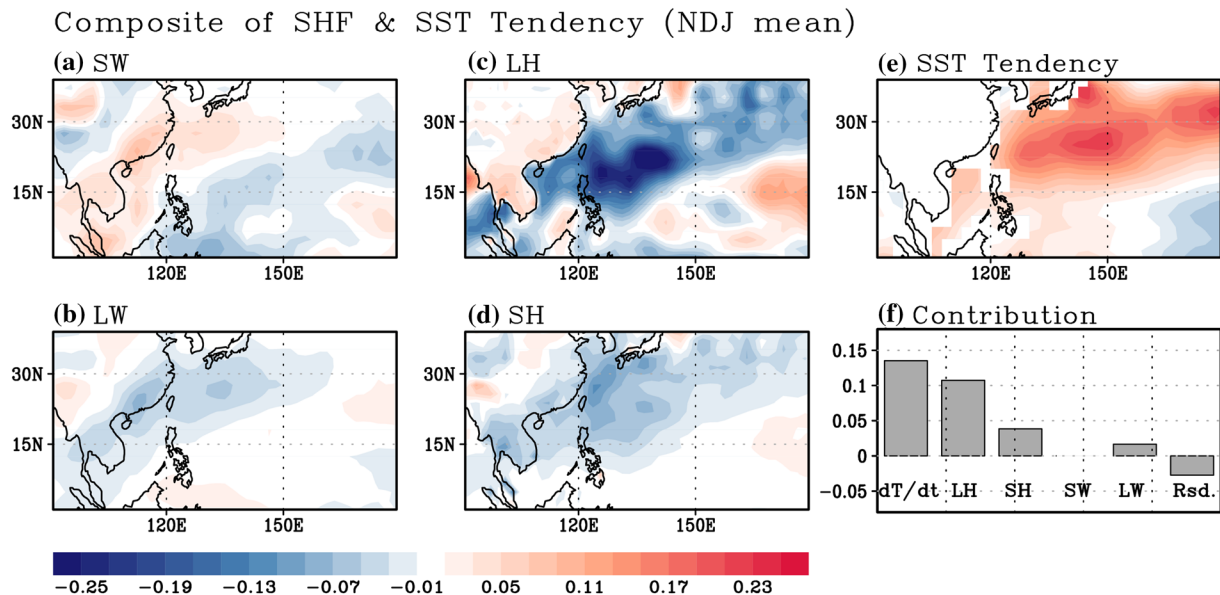


Fig. 2 Composite maps of anomalous surface heat fluxes and SST tendency during warm period of WNP mode. **a** Short wave, **b** long wave, **c** latent heat, **d** sensible heat, and **e** SST tendency (dsst/dt), respectively. Each flux is averaged from November to January (NDJ). Positive signs indicate upward heat flux from the surface. In **f**, the areal averaged SST tendency in NDJ season ($120\text{--}160^\circ\text{E}$, $15\text{--}30^\circ\text{N}$,

leftmost bar) and respective contributions from each heat fluxes (four middle bar) are indicated. The residual part (rightmost bar) which is difference between the SST tendency and the summation of the total contribution from surface heat fluxes indicates the contribution from oceanic dynamics

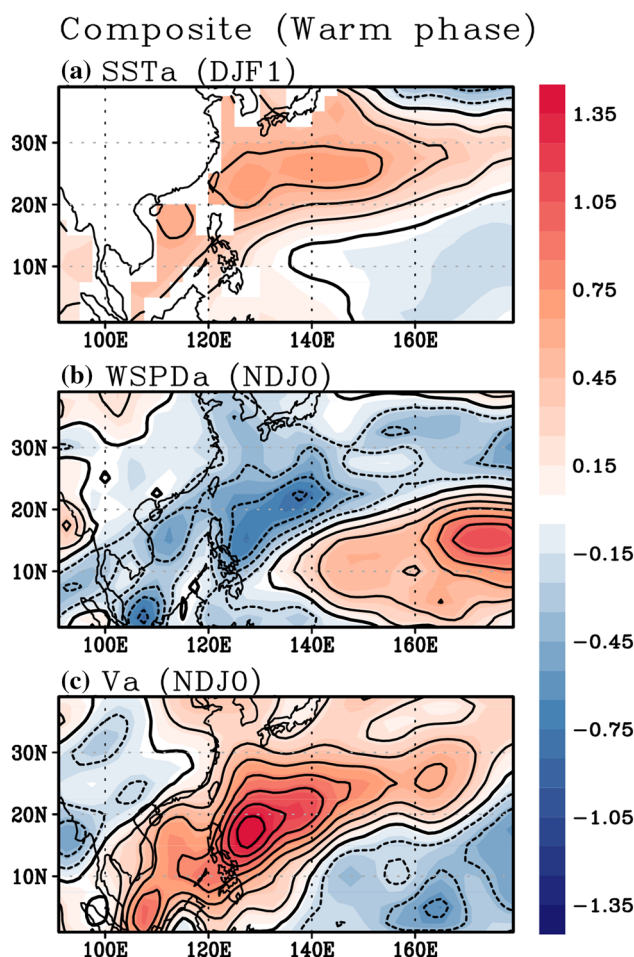


Fig. 3 Composite maps of **a** anomalous SST (DJF mean), **b** anomalous wind speed, and **c** anomalous meridional wind (NDJ mean) during warm period of WNP mode. Shading bar indicates the amplitude of the variables. Units are °C for SST and m/s for wind

specific humidity of the ocean surface and adjacent air at reference level, respectively.

Over the WNP, the climatological winter mean SST, wind speed, and atmospheric relative humidity adjacent to the ocean surface are approximately 25 °C, 10 m/s, and 90%, respectively. Under the assumption that the ocean surface is saturated with humidity and that relative humidity has small variation, changes in the latent heat flux due to the increased specific humidity differences associated with a 1 °C increase of surface temperature and 1 m/s decrease in wind speed are about 12 W/m² and -31 W/m², respectively, and their total effect (-19 W/m²) is comparable to the latent heat fluxes shown in Fig. 2c. This calculation indicates that latent heat flux changes through change by wind speed rather than by specific humidity effectively control the SST warming over the WNP. Here, 1 °C and 1 m/s increase or decrease in surface temperature and wind

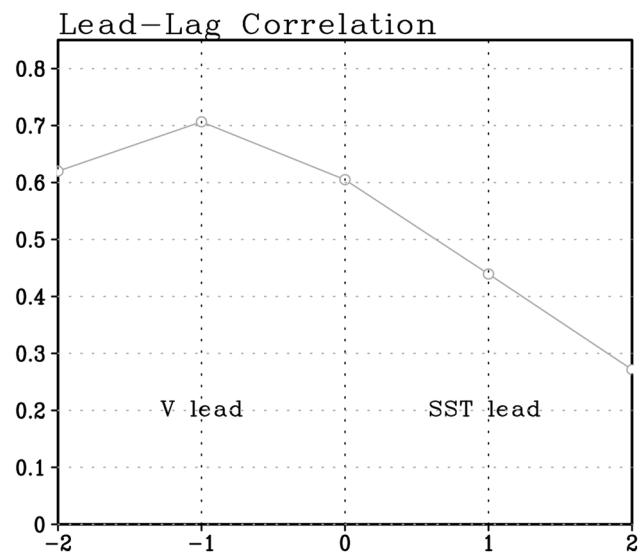


Fig. 4 Lead-lag correlation between SST and meridional wind anomalies over WNP region. Here, DJF means of averaged SST (110–150°E, 5–30°N) and wind (120–160°E, 5–30°N) are focused in the lead-lag relationship. X axis indicates lead-lag month, where minus means meridional wind leads SST, and vice versa. Y axis indicates correlation coefficients

speed with respect to the WNP mode are within their reasonable variation range.

Figure 3a–b shows the composite maps of DJF-mean SST and NDJ-mean wind speed anomalies. The pattern similarity between both composites implies that the SST anomaly is associated with the one-month-ahead reduced wind speed through latent heat flux change. To further understand this phenomenon, we checked the zonal and meridional winds separately, and we found that meridional wind anomalies play a dominant role in changing the wind speed over the WNP, as inferred from the resemblance of the wind speed pattern to the meridional wind pattern (Fig. 3c).

Since the northerly winds prevail climatologically over the WNP region during boreal winter, the anomalous southerly wind reduces the total wind speed. Then, less-than-normal latent heat fluxes through the weakened wind speed is expected to lead to ocean surface warming in situ, as shown in Fig. 3. A lead-lag relationship between the area-averaged meridional wind (120–160°E, 5–30°N) and SST (110–150°E, 5–30°N) anomalies over the WNP is clearly shown in Fig. 4, where the averaged region of winds is slightly displaced eastward compared with that of SST, since SST gradient rather than SST itself should be considered regarding generation of wind. In the calculation, DJF-mean is focused. For example, 1-month lead of meridional wind to the SST indicated the relationship between DJF-mean meridional wind and JFM-mean SST, and vice versa.

In the figure, the correlation coefficient, greater than 0.6, indicates the 95% confidence level, thus there exists simultaneous feedback between meridional wind and SST at zero lag. However, the higher coefficient at one-month lag indicates that the latent heat flux anomaly is essential in SST warming, and thus in the development of the WNP mode.

3.2 Wind–evaporation–SST (WES) feedback

As we discussed how the atmospheric fluxes induce SST anomalies, the ocean's feedback into atmospheric circulation is discussed in this section. As shown in Fig. 1a, the WNP mode has a SST warming center over the subtropical region between 20–30°N within 120–150°E, and the pattern occurs together with the low SLP located slightly northwest of the SST warming region, as shown in Fig. 5a. Meanwhile, the precipitation anomalies appear in the western region of the maximum SST axis in Fig. 5b. The precipitation composite is calculated by using the four recent warm phase years of the WNP mode after 1980 in Table 1, because of the short data period of GPCPv2.1. Precipitation anomalies imply atmospheric diabatic heating by latent heat release.

It is interesting that the pattern of SLP and wind relevant to the atmospheric heating inferred by the precipitation are similar to the Matsuno–Gill-type atmospheric response to the asymmetric atmospheric heating (Matsuno 1966; Gill 1980). Based on the Matsuno–Gill theory, off-equatorial atmospheric heating induces low SLP in the northwestern region of the atmospheric heating because of the increased Rossby and reduced Kelvin wave effects, and accordingly, southerly wind becomes dominant over the atmospheric heating region (Fig. 5, vector).

The anomalous southerly wind induced by the SST and its related atmospheric heating completes the

wind–evaporation–SST (WES) feedback (Xie and Philander 1994) over the WNP. To summarize the WES feedback, the reduced wind speed generated by anomalous southerly winds induces SST warming through less-than-normal latent heat flux at the ocean surface. The anomalous SST and associated precipitation anomalies enhance the anomalous southerly wind via the Matsuno–Gill-type atmospheric response to the diabatic heating, which reduces the wind speed even more (Fig. 6). As a result of the WES feedback, the WNP mode can be developed and maintained during the boreal winter season until the northerly mean wind disappears in boreal spring. Here, it is noted that such WES feedback over the WNP is distinguished from that over the equatorial western Pacific explained in Ueki (2011) in which WES feedback is associated to the hemispheric SST gradient.

◆ Wind–Evaporation–SST (WES) Feedback

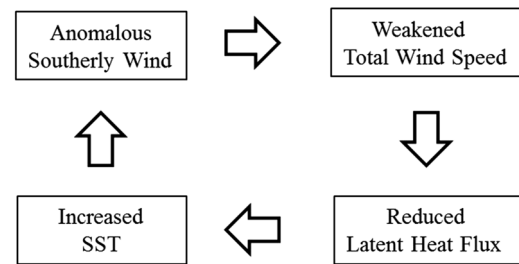


Fig. 6 Diagram of WES feedback over WNP region during winter

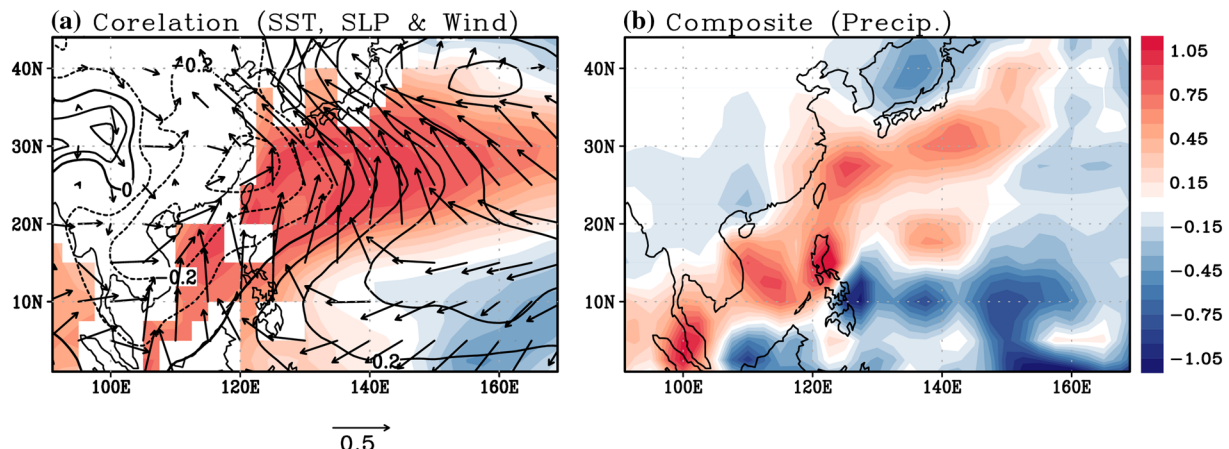


Fig. 5 **a** Correlation map of SST (shading), SLP (contours), and wind (vectors) based on WNP index during boreal winter. **b** Composite of precipitation of warm periods of WNP mode (mm/day)

4 Atmospheric teleconnection toward North Pacific/North America

In the regression maps of geopotential height at 500 hPa and SLP against the WNP index (Fig. 7a–b), it is found that the north–south dipole pattern with a barotropic structure is located over the North Pacific, and the spatial structures have much in common with the western Pacific oscillation (WPO) and NPO patterns (e.g., Wallace and Gutzler 1981; Linkin and Nigam 2008). It is well known that the surface heat fluxes modified by the NPO-related surface wind stresses induce NPGO featured by the north–south tripole SST pattern over the North Pacific.

The WNP mode has a significant relationship with the geopotential height and SLP over North America, as well as those over the North Pacific, which shows an east–west pressure contrast over North America. According to Hartmann (2015), such east–west pressure displacement with opposite phase in Fig. 7 (i.e., cold phase of WNP mode) could cause a cold surge over the eastern part of North America. Finally, these results suggest a strong possibility that the variability of the WNP mode is closely related to the climate over the North Pacific and North America. Here, we further investigate the influence of the WNP mode on the climate over the North Pacific and North America, particularly focusing on NPO generation mechanisms and possible causes of cold weather over eastern North America.

To investigate the atmospheric vertical structure of the WNP mode over the WNP region, here we compute the regression of upper and lower level divergences and mid-troposphere vertical velocity against the WNP index. As shown in Fig. 8a, the strong low-level convergence appears in the northern region of the maximum axis of the southerly wind (Fig. 3c), which indicates that the low-level convergence results from the strong inflow of the southerly wind. It is noted that the anomalous southerly wind plays a

role in enhancing diabatic heating by driving the low-level convergence in addition to increasing SST. This diabatic heating induces mid-level upward motion (Fig. 8c), which is vertically connected to the upper-level atmosphere, so that strong upper-level divergence is located in the southern part of Korea and Japan (Fig. 8b).

It is likely that the upward motion expands the local Hadley circulation further northward (Fig. 9a). At this point, because of the dynamical linkage between the northern edge of local Hadley circulation and upper-level jet stream (Park and An 2014), the East Asian jet is moved northward as well (Fig. 9b). It should be noted that such modulation of local Hadley circulation and jet location accompanies relative vorticity change there.

Such divergence (i.e., divergent flow) and vorticity change in the upper-level atmosphere as shown above are closely related to the initial process of atmospheric teleconnection. In order to diagnose the atmospheric teleconnection, here we use the Rossby wave source (RWS) equation (Sardeshmukh and Hoskins 1988):

$$\text{RWS} = -\nabla \cdot (\overrightarrow{V}_x \zeta) \quad (2)$$

where \overrightarrow{V}_x and ζ are a divergent wind vector (i.e., wind caused by the velocity potential) and absolute vorticity, respectively. The equation indicates that the divergence of vorticity flux contributes to the generation of the RWS. Through linearization of Eq. (2), the anomalous RWS equation is divided into two terms:

$$\text{RWS}' \cong -\nabla \cdot (\overrightarrow{V}_x' \zeta) - \nabla \cdot (\overline{\overrightarrow{V}_x} \zeta') \quad (3)$$

The first and second terms indicate the RWS generation induced by the anomalous divergence flow and by the anomalous absolute vorticity, respectively. The total and each RWS term in Eq. (3) are regressed against the WNP index (Fig. 10). From the calculation, it is seen that the

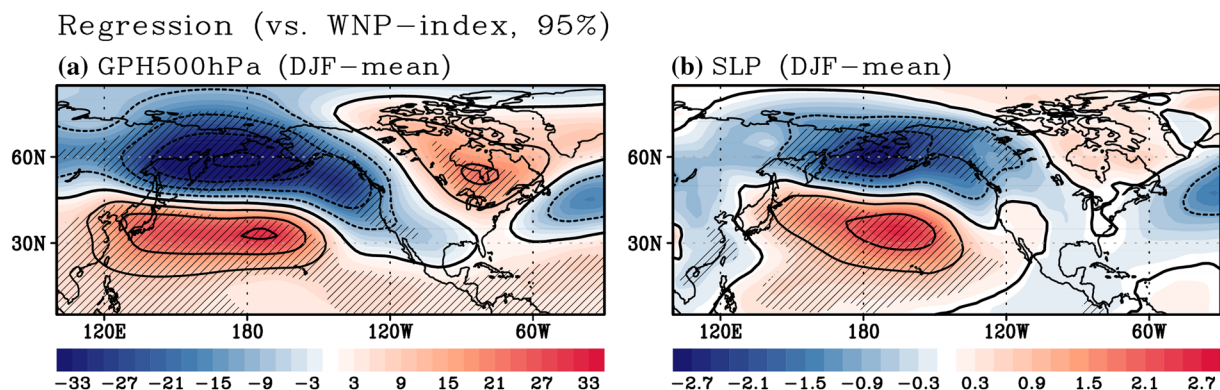


Fig. 7 Regression maps of DJF-mean geopotential height at 500 hPa (a) and SLP (b) against WNP index; 95% confidence level is indicated by hatching

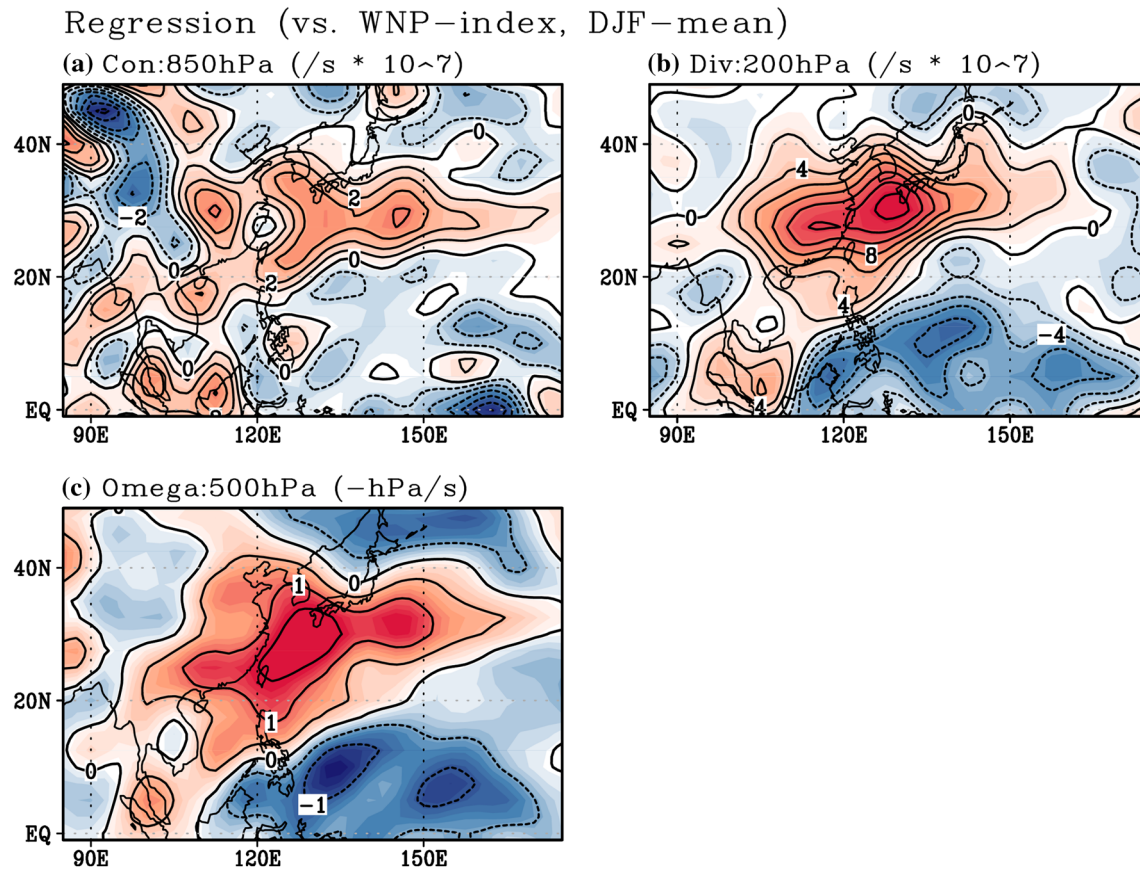


Fig. 8 Regression maps of DJF-mean **a** low-level divergence, **b** upper-level divergence, and **c** velocity pressure (omega) at 500 hPa against WNP index. Units are indicated in the figure

influence of the anomalous divergent flow (Fig. 10b) on the generation of the RWS is comprehensively dominant. However, the anomalous vorticity modulation effect induced by the meridional circulation change is not negligible near the East Asian jet region (Fig. 10c). As a result of both effects, a strong RWS is developed in the southern part of Korea and Japan.

Based on the RWS, the excited atmospheric waves propagate toward the downstream regions. To understand the direction of the wave propagation, the wave activity flux (WAF) analysis suggested by Takaya and Nakamura (2001) is examined. It is shown that the WAF divides toward the northern and southern regions of the North Pacific and escapes to North America (Fig. 11). Such WAF is consistent with the NPO-like dipole pressure pattern over the North Pacific (Fig. 7), which in turn modifies the surface heat flux, leading to the NPGO-like SST pattern. This result indicates that the WNP mode remotely controls the North Pacific climate.

It should be noted that such wave propagation is connected further to North America. From this wave propagation, the east–west pressure contrast over North America

is displaced. As mentioned above, such east–west pressure configuration causes cold weather over eastern North America by inducing cold air intrusion there. It is also suggested that the NPGO-like SST pattern over the North Pacific contributes to the cold weather over eastern North America (Hartmann 2015). Therefore, it is reasonably concluded that the WNP mode plays an important role even in the North America climate both directly by atmospheric teleconnection and indirectly by SST modulation over the North Pacific. This result is well proven by that the recent cold winters over the eastern North America during 2014 and 2015 winter are well matched to the cold periods of the WNP mode as indicated in Table 2.

For further confirmation of the atmospheric teleconnection from the WNP mode, a linear baroclinic model (LBM) experiment (Watanabe and Kimoto 2000) is constructed. In the experiment, the winter-mean atmospheric climatology during 1955–2015 is used as the atmospheric background, and for the mid-level atmospheric heat forcing the upward motion over the WNP (Fig. 8c), ranging 105–140°E within 20–40°N, is taken (Fig. 12a). It is assumed that upward motion represents precipitation, thus latent heat release into

Fig. 9 Composite (black contours) of **a** DJF-mean stream function and **b** zonal wind during warm period of WNP mode. Red contours indicate climatology. Shading indicates their difference (composite minus climatology)

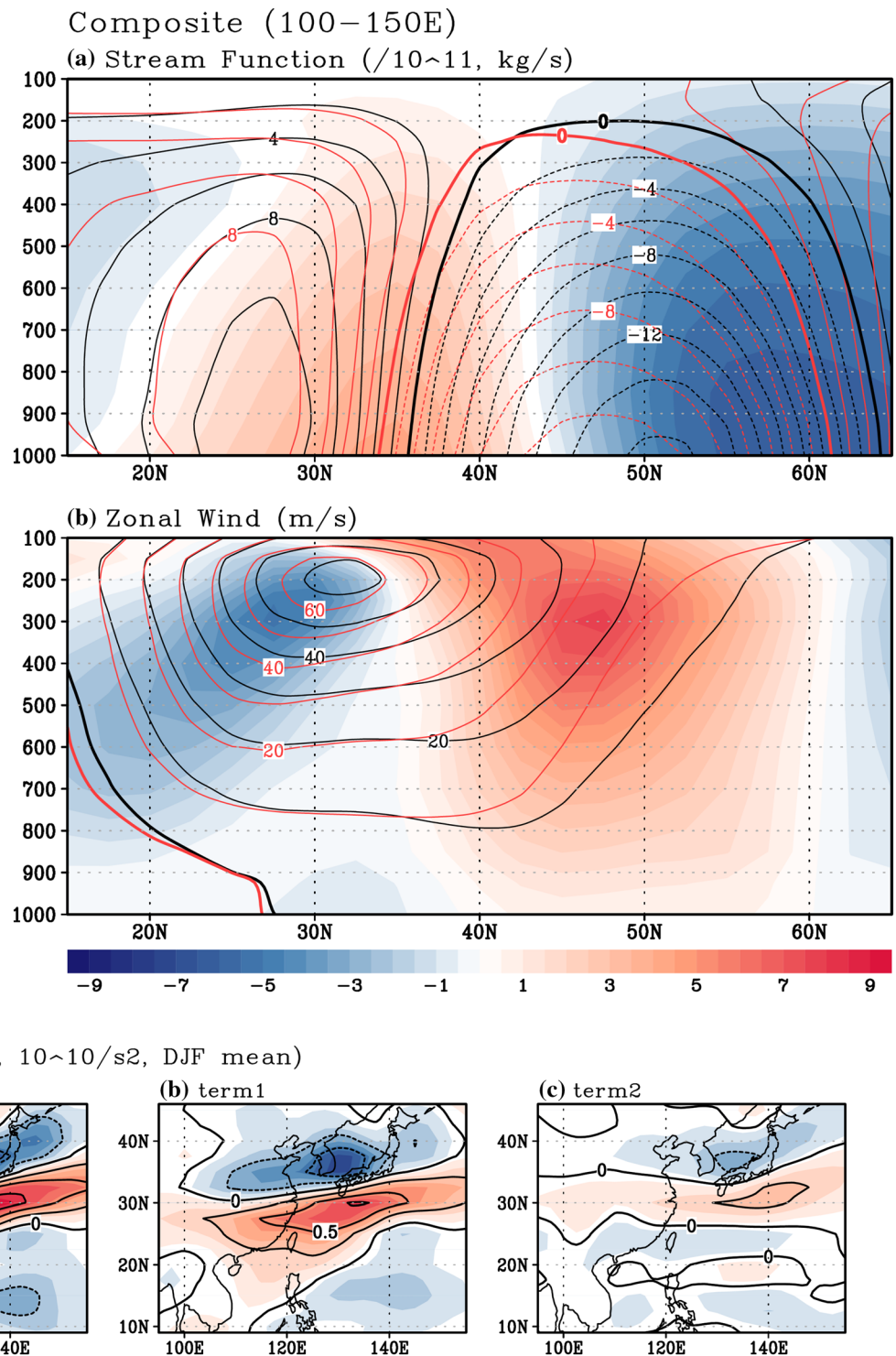
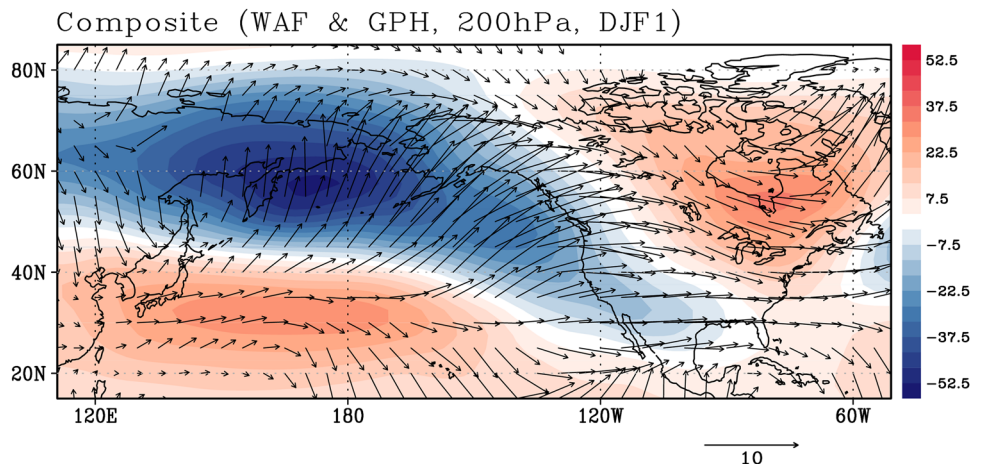


Fig. 10 Regression maps of DJF-mean Rossby wave sources (RWS) against WNP index: **a** total; **b** term 1; **c** term 2

the atmosphere. Figure 12b, c show the steady atmospheric responses to the heating forcing based on the atmospheric background, obtained from the last 10-day average from the total 30-day run. At the geopotential height of 500 hPa, wave propagation toward the North Pacific and to North

America initiated by the WNP is clearly seen. Here, the ridge over the eastern North Pacific seems to be induced by the Rossby wave propagation (Hoskins and Ambrizzi 1993) trapped by the Pacific jet stream, and the trough near the Bering Sea seems to be the result of a Rossby wave

Fig. 11 Composite maps of DJF-mean geopotential height (shading) and wave activity flux (WAF, vector) based on warm period of WNP mode



LBM experiment (1955–2015, Dec–Feb)

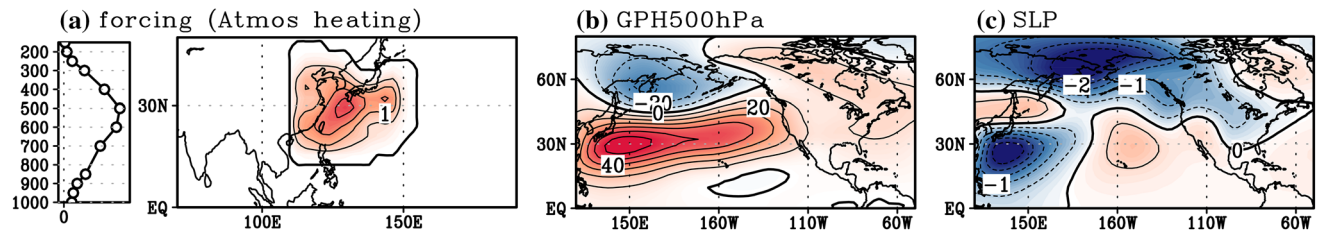


Fig. 12 Forcing and steady response of LBM experiment. **a** Solid line in leftmost panel indicates the vertical weighting of the horizontal heating forcing pattern (right panel) which follows the omega pattern during warm period of WNP mode and its steady atmospheric response for **b** GPH at 500 hPa and **c** SLP. The contour intervals are 0.5 °C, 10 m and 0.5 hPa, respectively

pattern during warm period of WNP mode and its steady atmospheric response for **b** GPH at 500 hPa and **c** SLP. The contour intervals are 0.5 °C, 10 m and 0.5 hPa, respectively

train tracking a great circle toward high latitudes from the WNP (Hoskins and Karoly 1981). As a result of the wave propagation, the north–south dipole pattern (NPO) over the North Pacific and the east–west pressure contrast over North America can be displaced.

5 Summary and discussion

We proposed a mechanism for the interannual variations of the SST anomalies over the WNP and analyzed their atmospheric teleconnection toward the North Pacific/North America. First, the WNP mode, featuring SST warming over the subtropical region, is defined as the first EOF mode of SST anomalies over the WNP. We found that anomalous southerly wind plays an essential role for the development of the WNP mode in the presence of climatological northerly background wind over the WNP during boreal winter. The anomalous southerly wind reduces the total wind speed over the WNP, which results in less-than-normal latent heat flux from the ocean surface. As a result, SST increases over the WNP. At the same time, the atmospheric response to the SST warming and its related

atmospheric heating further enhances the southerly wind anomaly over the WNP. In such a way, wind–evaporation–SST (WES) feedback operates strongly, and the WNP mode is developed and maintained throughout the boreal winter until the following spring when the prevailing climatological northerly wind started to be weaker.

We revealed that the atmospheric teleconnection associated with the WNP mode toward the extratropical region can produce an NPO-like structure over the North Pacific, which has not been clearly explained before, although some studies have mentioned that the NPO is caused by the atmospheric teleconnection from the tropics (Park et al. 2012). With regard to the atmospheric teleconnection, we found that upper-level divergence in the southern part of the Korean Peninsula is important for the related teleconnections. The upper-level divergence contributes to the generation of the strong RWS in the same region. In turn, RWS-excited waves can propagate to the downstream regions, producing an NPO-like pressure pattern. This result supports a significantly high correlation between the WNP mode and NPO. We also found that the teleconnections associated with the WNP mode exist not only in the North Pacific but also in North America. The featured

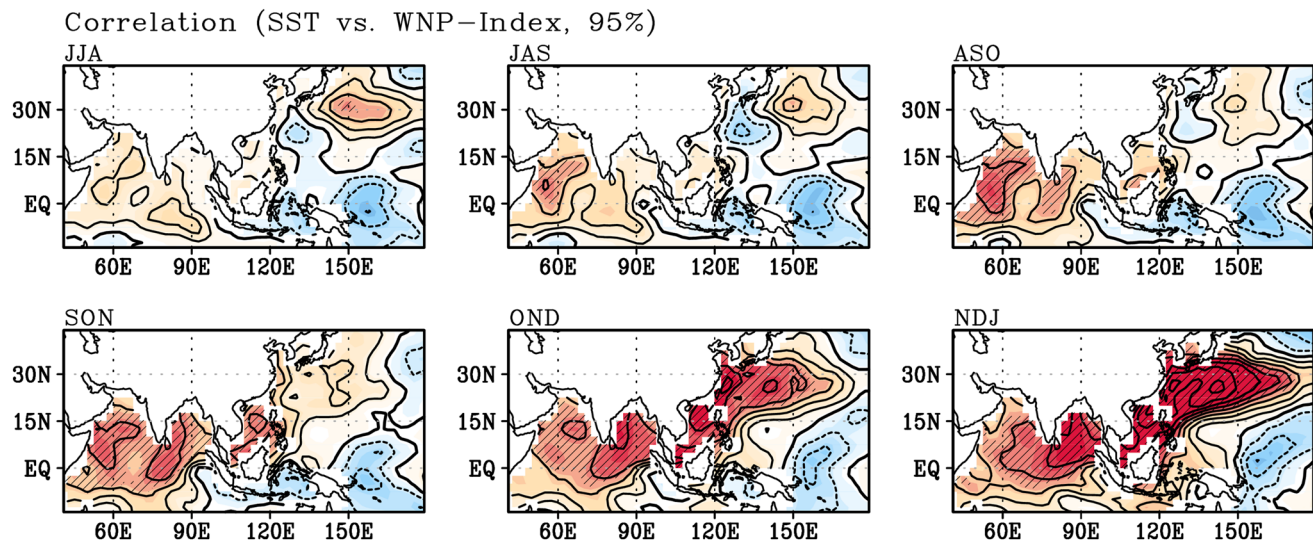


Fig. 13 Lead-lag correlation maps of 3-month averaged SST anomalies based on the WNP index. Above all panels indicate preceding SST patterns of WNP mode. Shading indicates 95% confidence level and contour intervals are 0.1

zonal contrast patterns of mid-level geopotential and SLP over North America tend to lead to a favorable condition for bringing cold air into North America.

There exist well-known atmospheric teleconnection patterns over the North Pacific to North America regions such as western Pacific oscillation (WPO) and Pacific-North America (PNA) (Horel and Wallace 1981; Wallace and Gutzler 1981), hence it is needed to consider what atmospheric teleconnection patterns are related to the WNP mode. Over the western to central North Pacific sector, western Pacific oscillation (WPO) featured by north-south dipole is present, of which pattern has a similarity the WNP-mode related atmospheric pattern as shown in Fig. 7a. As a result, it is thought that WNP mode has to do with WPO. Indeed, because WPO is frequently considered as the 500 hPa level-manifestation of NPO as suggested in Linkin and Nigam (2008), the interpretation that WPO is related to WNP mode is reasonable. On the other hand, over the eastern Pacific to North America sector, Pacific-North America (PNA) pattern characterized by meridionally spread three action centers over the region is famous. However, such meridional fluctuated atmospheric pattern is apparently different from the east–west contrast pattern as shown in Fig. 7a, thus it is said that the WNP-related atmospheric pattern is totally different from PNA.

As we showed in this study, WNP mode has its own developing mechanism and its atmospheric teleconnection strongly influences the North Pacific climate more than CP-El Niño. Actually, the correlation coefficient between CP-El Niño index which is used in Table 1 and NPGO index is 0.42 (0.30 for El Niño Modoki index from Ashok et al. 2007) which is quite smaller than the

correlation between WNP mode and NPGO of 0.69 as shown in Table 1. Therefore, it implies that WNP mode rather than CP-El Niño may be more climatologically related to the North Pacific.

Because the WNP mode has significant impacts on the extratropical circulation over the Northern Hemisphere, it is important to know whether or not the WNP mode is predictable. In other words, it is important to understand how the WNP mode can be triggered. Based on the sequential lead-lag correlation between SST and the WNP index, we found that the northern Indian Ocean warming during the previous summer to fall season is followed by the WNP mode (Fig. 13). The warming signal over the northern Indian Ocean is connected to the South China Sea in the following fall season, which seems to be a possible starting point for the WES feedback, and therefore the WNP mode during the boreal winter season. This implies the crucial role of the Indian Ocean in the North Pacific climate, with a time lag. The influence of the Indian Ocean on the WNP mode should be investigated in detail in a further study.

Acknowledgements This work was supported by the Korea Meteorological Administration Research and Development Program under Grant KMIPA 2015-1043.

References

- Ashok K, Behera SK, Rao SA et al (2007) El Niño Modoki and its possible teleconnection. *J Geophys Res Oceans* 112:C11007. doi:10.1029/2006JC003798

- Bond N, Overland J, Spillane M et al (2003) Recent shifts in the state of the North Pacific. *Geophys Res Lett* 30:2183. doi:[10.1029/2003GL018597](https://doi.org/10.1029/2003GL018597)
- Ceballos LI, Di Lorenzo E, Hoyos CD et al (2009) North Pacific gyre oscillation synchronizes climate fluctuations in the eastern and western boundary systems. *J Clim* 22:5163–5174. doi:[10.1175/2009JCLI2848.1](https://doi.org/10.1175/2009JCLI2848.1)
- Chhak KC, Di Lorenzo E, Schneider N et al (2009) Forcing of low-frequency ocean variability in the Northeast Pacific. *J Clim* 22:1255–1276. doi:[10.1175/2008JCLI2639.1](https://doi.org/10.1175/2008JCLI2639.1)
- Chikamoto Y, Timmermann A, Luo J-J et al (2015) Skilful multi-year predictions of tropical trans-basin climate variability. *Nat Commun* 6:6869. doi:[10.1038/ncomms7869](https://doi.org/10.1038/ncomms7869)
- Di Lorenzo E, Schneider N, Cobb K et al (2008) North Pacific Gyre Oscillation links ocean climate and ecosystem change. *Geophys Res Lett* 35:L08607
- Di Lorenzo E, Cobb KM, Furtado JC et al (2010) Central Pacific El Niño and decadal climate change in the North Pacific Ocean. *Nature Geosci* 3:762–765. doi:[10.1038/ngeo984](https://doi.org/10.1038/ngeo984)
- Fu R, Del Genio AD, Rossow WB (1994) Influence of ocean surface conditions on atmospheric vertical thermodynamic structure and deep convection. *J Clim* 7:1092–1108
- Gill AE (1980) Some simple solutions for heat-induced tropical circulation. *Q J R Meteorol Soc* 106:447–462
- Hartmann DL (2015) Pacific sea surface temperature and the winter of 2014. *Geophys Res Lett* 42:1894–1902
- Horel JD, Wallace JM (1981) Planetary-scale atmospheric phenomena associated with the Southern Oscillation. *Mon Wea Rev* 109: 813–829
- Hoskins BJ, Ambrizzi T (1993) Rossby wave propagation on a realistic longitudinally varying flow. *J Atmos Sci* 50:1661–1671
- Hoskins BJ, Karoly DJ (1981) The steady linear response of a spherical atmosphere to thermal and orographic forcing. *J Atmos Sci* 38:1179–1196
- Hu D, Cui M (1991) The western boundary current of the Pacific and its role in the climate. *Chin J Oceanol Limn* 9:1–14
- Huffman GJ, Adler RF, Bolvin DT et al (2009) Improving the global precipitation record: GPCC version 2.1. *Geophys Res Lett* 36:L17808. doi:[10.1029/2009GL040000](https://doi.org/10.1029/2009GL040000)
- Jo H-S, Yeh S-W, Kirtman BP (2014) Role of the western tropical Pacific in the North Pacific regime shift in the winter of 1998/1999. *J Geophys Res. Oceans* 119:6161–6170
- Kao H-Y, Yu J-Y (2009) Contrasting eastern-Pacific and central-Pacific types of ENSO. *J Clim* 22:615–632
- Kara AB, Rochford PA, Hurlburt HE (2003) Mixed layer depth variability over the global ocean. *J Geophys Res. Oceans* 108:3079. doi:[10.1029/2000JC000736](https://doi.org/10.1029/2000JC000736)
- Kistler R, Collins W, Saha S et al (2001) The NCEP–NCAR 50-year reanalysis: monthly means CD-ROM and documentation. *Bull Amer Meteor Soc* 82:247–267
- Kug J-S, Jin F-F, An S-I (2009) Two types of El Niño events: cold tongue El Niño and warm pool El Niño. *J Clim* 22:1499–1515
- Larkin NK, Harrison D (2005) On the definition of El Niño and associated seasonal average US weather anomalies. *Geophys Res Lett* 32: L13705. 1–L13705. 4
- Lee S-K, Park W, Baringer MO et al (2015) Pacific origin of the abrupt increase in Indian Ocean heat content during the warming hiatus. *Nature Geosci* 8:445–449
- Linkin ME, Nigam S (2008) The North Pacific oscillation–West Pacific teleconnection pattern: mature-phase structure and winter impacts. *J Clim* 21:1979–1997
- Mantua NJ, Hare SR, Zhang Y et al (1997) A Pacific interdecadal climate oscillation with impacts on salmon production. *Bull Amer Meteor Soc* 78:1069–1079
- Matsuno T (1966) Quasi-geostrophic motions in the equatorial area. *J Meteor Soc Japan* 44:25–43
- Park J-H, An S-I (2014) The impact of tropical western Pacific convection on the North Pacific atmospheric circulation during the boreal winter. *Clim Dyn* 43:2227–2238
- Park J-Y, Yeh S-W, Kug J-S (2012) Revisited relationship between tropical and North Pacific sea surface temperature variations. *Geophys Res Lett* 39:L02703. doi:[10.1029/2011GL050005](https://doi.org/10.1029/2011GL050005)
- Reynolds RW, Smith TM, Liu C et al (2007) Daily high-resolution-blended analyses for sea surface temperature. *J Clim* 20:5473–5496
- Rogers JC (1981) The North Pacific Oscillation. *J Clim* 1:39–57
- Sardeshmukh PD, Hoskins BJ (1988) The generation of global rotational flow by steady idealized tropical divergence. *J Atmos Sci* 45:1228–1251
- Takaya K, Nakamura H (2001) A formulation of a phase-independent wave-activity flux for stationary and migratory quasigeostrophic eddies on a zonally varying basic flow. *J Atmos Sci* 58:608–627
- Toole JM, Millard RC, Wang Z et al (1990) Observations of the Pacific North equatorial current bifurcation at the Philippine coast. *J Phys Oceano* 20:307–318
- Ueki I (2011) Evidence of wind-evaporation-sea surface temperature (WES) feedback in the western Pacific warm pool during the mature phase of the 1997–98 El Niño. *Geophys Res Lett* 38:L11603. doi:[10.1029/2011GL047179](https://doi.org/10.1029/2011GL047179)
- Wallace JM, Gutzler DS (1981) Teleconnections in the geopotential height field during the Northern Hemisphere winter. *Mont Weather Rev* 109:784–812
- Wang B, Wu R, Fu X (2000) Pacific-East Asian teleconnection: how does ENSO affect East Asian climate? *J Clim* 13:1517–1536
- Watanabe M, Kimoto M (2000) Atmosphere-ocean thermal coupling in the North Atlantic: a positive feedback. *Q J R Meteorol Soc* 126:3343–3369
- Xie SP, Philander SGH (1994) A coupled ocean-atmosphere model of relevance to the ITCZ in the eastern Pacific. *Tellus A* 46:340–350
- Yu JY, Kao HY (2007) Decadal changes of ENSO persistence barrier in SST and ocean heat content indices: 1958–2001. *J Geophys Res Atmos* 112:13106
- Zhang C (1993) Large-scale variability of atmospheric deep convection in relation to seasurface temperature in the tropics. *J Clim* 6:1898–1913